

Non-Newtonian fluid flow through three-dimensional disordered porous media

Apiano F. Morais¹, Hansjoerg Seybold², Hans J. Herrmann^{1,2} and José S. Andrade Jr.^{1,2}

¹*Departamento de Física, Universidade Federal do Ceará, 60451-970 Fortaleza, Ceará, Brazil*

²*Computational Physics, IFB, Schafmattstr. 6, ETH, 8093 Zurich, Switzerland*

(Dated: May 30, 2018)

We investigate the flow of various non-Newtonian fluids through three-dimensional disordered porous media by direct numerical simulation of momentum transport and continuity equations. Remarkably, our results for power-law (PL) fluids indicate that the flow, when quantified in terms of a properly modified permeability-like index and Reynolds number, can be successfully described by a single (universal) curve over a broad range of Reynolds conditions and power-law exponents. We also study the flow behavior of Bingham fluids described in terms of the Herschel-Bulkley model. In this case, our simulations reveal that the interplay of (i) the disordered geometry of the pore space, (ii) the fluid rheological properties, and (iii) the inertial effects on the flow is responsible for a substantial enhancement of the macroscopic hydraulic conductance of the system at intermediate Reynolds conditions. This anomalous condition of “enhanced transport” represents a novel feature for flow in porous materials.

PACS numbers: 47.56.+r, 64.60.ah, 47.50.-d, 47.11.-j

The research on flow through porous media has great relevance for many problems of practical interest in several fields, including physics, medicine, biology, chemical and mechanical engineering and geology [1, 2, 3]. The disordered aspect of most natural and artificial porous materials is directly responsible for the presence of local flow heterogeneities that can dramatically affect the behavior, for example, of the transport of heat and mass through the system. Under this framework, the standard approach to investigate single-phase flow in porous media is to apply Darcy’s law [1, 2, 3], which simply assumes that a global permeability k relates the average fluid velocity u_0 in the field with the pressure drop Δp measured across the system,

$$u_0 = -\frac{k}{\mu} \frac{\Delta p}{L}, \quad (1)$$

where L is the length of the sample in flow direction and μ is the viscosity of the fluid. As a macroscopic index, the permeability reflects the relation between the complex pore space morphology and fluid flow.

In previous studies [4, 5, 6, 7, 8, 9, 10], detailed models of pore geometry have been used in combination with computational fluid dynamics simulations to predict permeability coefficients and validate classical semi-empirical correlations for real porous materials. In principle, the original concept of permeability as a global index for flow in porous media, however, is only applicable in the limit of Stokesian flow (linear). Strictly speaking, the validity of Darcy’s law should be restricted to (i) Newtonian fluids and (ii) flows under viscous conditions, i.e., flows at very low Reynolds numbers, defined usually as $\text{Re} \equiv \rho u_0 d_p / \mu$, where ρ is the density of the fluid and d_p is the grain diameter. The departure from Darcy’s law due to the contribution of inertial forces (convection) to the flow of Newtonian fluids has been the subject of several studies in the past [10, 11, 12]. In particular, it has

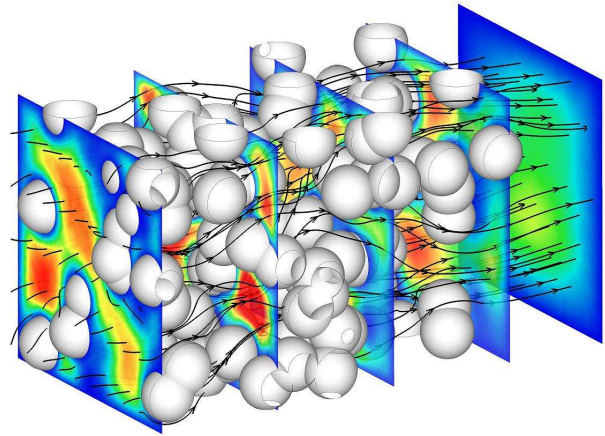


FIG. 1: (Color online) Non-Newtonian (power-law) fluid flow through a typical realization of the Swiss-Cheese pore space ($\varepsilon = 0.7$). The fluid is pushed from left to right. The solid lines with arrows correspond to trajectories of tracer particles released in the flow, while the contour plots give the velocity magnitude at different cross-sections of the porous medium. Their colors ranging from blue (dark) to red (light) correspond to low and high velocity magnitudes, respectively.

been experimentally and numerically observed that the breakdown of condition (ii) can take place even under laminar flow conditions, i.e., before fully developed turbulence effects become relevant to momentum transport.

In order to understand the physics of important problems like blood flow through the kidney [13] or oil flow through porous rocks [14], for example, one has to overcome the restriction (i) mentioned above by explicitly considering the nonlinear behavior of these fluids under shear, namely, their specific non-Newtonian properties. Although these fluids have been known for a long time, technological applications which directly make use of their anomalous rheological behavior have come into

focus only recently. For instance, shear thinning solvents are present in droplets paints [15], and shear thickening fluids are currently used as active dampers and components of enhanced body armors [16]. While the physical properties of Newtonian fluid flow through irregular media are theoretically well understood and have been confirmed by many experiments, non-Newtonian systems [17, 18, 19] lack a generalized description. In this Letter we investigate the flow of non-Newtonian fluids through three-dimensional porous media by direct numerical simulation of momentum and continuity equations. To the best of our knowledge, this is the first time that non-linear effects coming from both rheological and inertial aspects of the fluid flow are considered simultaneously in the framework of a disordered three-dimensional pore space.

The porous medium studied here is a three-dimensional realization of the Swiss-Cheese model [20]. Spherical particles (solid obstacles) of diameter d_p are sequentially and randomly placed in a box of length L in the x -direction and square cross-section of area A . Particle overlap is allowed and the allocation process continues up to the point in which a prescribed value for the porosity (void fraction) ε is achieved. The mathematical formulation for the fluid mechanics in the interstitial pore space is based on the assumptions that we have a continuum and incompressible fluid flowing under steady-state and isothermal conditions. Thus, the momentum and mass conservation equations reduce to,

$$\rho \vec{u} \cdot \nabla \vec{u} = -\nabla p + \nabla \mathcal{T} \quad (2)$$

$$\nabla \cdot \vec{u} = 0, \quad (3)$$

where \vec{u} and p are the velocity and pressure fields, respectively, and \mathcal{T} is the so-called deviatoric stress tensor given by,

$$\mathcal{T}_{ij} = 2\mu \dot{s}_{ij}, \quad (4)$$

where $\dot{s}_{ij} = \frac{1}{2} \left(\frac{\partial u_i}{\partial x_j} + \frac{\partial u_j}{\partial x_i} \right)$ is the strain rate tensor. The variable μ is the dynamic viscosity, for which a constitutive relation must be provided in order to describe the specific non-Newtonian behavior of the fluid. Here we investigate the flow of two different types of rheologies, namely, the cross-power-law fluid and the Bingham fluid. The constitutive relation for a PL fluid can be written as,

$$\mu = K \dot{\gamma}^{n-1}, \quad \mu_1 < \mu < \mu_2, \quad (5)$$

where the constants μ_1 and μ_2 are the lower and upper cutoffs, $\dot{\gamma} \equiv \sqrt{\frac{1}{2} \dot{s}_{ij} \dot{s}_{ij}}$ is the effective strain rate, K is the consistency index, and n is the power-law exponent. For $n = 1$ we recover the behavior of a Newtonian fluid. Fluids with $n > 1$ are shear-thickening, while shear-thinning behavior corresponds to $n < 1$.

In the case of Bingham fluids, the rheology is commonly approximated by the Herschel-Bulkley model [21,

22] which combines the effects of Bingham and power-law behavior for a fluid. For low strain rates, $\dot{\gamma} < \tau_0/\mu_0$, the material acts as a very viscous fluid with viscosity μ_0 . As the strain rate increases and the yield stress threshold τ_0 is surpassed, the fluid behavior is described by,

$$\mu = \frac{\tau_0 + K_B [\dot{\gamma}^n - (\tau_0/\mu_0)^n]}{\dot{\gamma}}, \quad (6)$$

where K_B is the consistency factor and n is the power-law index. Here we restrict our simulations to the case of Bingham fluids $n = 1$, i.e., the fluid is still Newtonian at large strain rates, with a viscosity $\mu = K_B$.

Non-slip boundary conditions are applied along the entire solid-fluid interface and end effects on the flow field, which become significant at high Reynolds numbers, are minimized by attaching ancillary zones at the inlet and outlet of the two opposite faces in the direction of the flow (i.e., x -direction). At the inlet, a constant inflow velocity in the normal direction to the boundary is specified, whereas at the outlet we impose gradientless boundary condition. Finally, the four remaining faces are considered to be solid walls.

For a given realization of the porous medium and a given set of flow and constitutive parameters of the fluid, the numerical solution of the partial differential equations (2) for the local velocity and pressure fields in the fluid phase of the void space, head and recovery zones is obtained by discretization using the control volume finite-difference technique [23]. An unstructured grid with up to three million tetrahedral cells is adapted to the geometry of the porous medium. For comparison, entirely consistent numerical solutions have also been calculated with a finite-volume scheme [24]. Finally, from the area-averaged pressures at the inlet and outlet positions, the overall pressure drop can be readily calculated.

In Fig. 1 we show a three-dimensional plot of a typical realization of the porous medium through which a power-law fluid flows. Clearly, the complex geometry of the pore space induces preferential channels on the flow whose localization and strength are significantly dependent on the rheological properties of the fluid as well as on the imposed inlet-outlet boundary conditions. For PL fluids, this intricate interplay between geometry and flow can nevertheless be macroscopically quantified in terms of an analogous to a permeability index, namely a hydraulic conductivity, defined in terms of Darcy's law as $k_D \equiv K_1 u_0 L / \Delta p$, where K_1 is a reference viscosity taken as the consistency index for $n = 1$. As shown in the inset of Fig. 2, the general behavior of k_D is qualitatively similar for different values of the exponent n . Moreover, it follows the characteristic trend of a simple Newtonian fluid ($n = 1$), namely that k_D remains essentially invariant for low Re values up to a crossover point Re_\times where it starts to decrease due to the onset of non-linear convective effects on the flow [7, 10, 25]. Quantitatively,

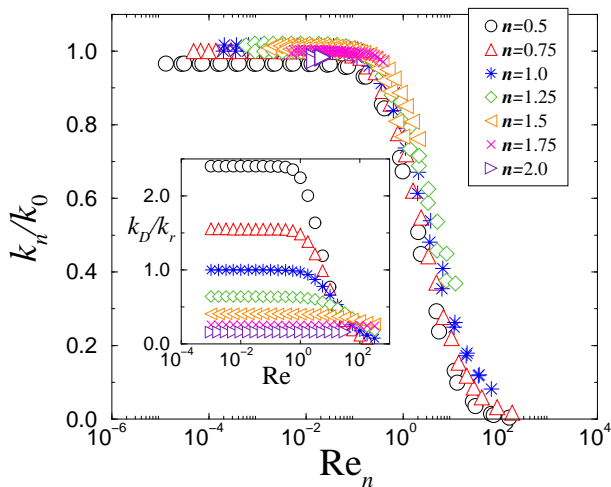


FIG. 2: (Color online) Flow of power-law fluids through three-dimensional porous media. The inset shows the variation of the ratio k_D/k_r with Reynolds number $Re \equiv \rho u_0 d_p / K_1$ for different values of the power-law exponent n and $\varepsilon = 0.5$. The resulting data collapse presented in the main plot confirms the adequacy of our rescaling procedure in terms of the modified permeability index k_n/k_0 and the modified Reynolds number Re_n (see text).

however, we observe that both the upper limit for k_D and Re_x are strongly dependent on n .

Darcy's law has been generalized to power-law fluids in previous studies [26, 27, 28]. Here we define an hydraulic conductivity as,

$$k_n \equiv u_0 K \left(\frac{\Delta p}{L} \right)^{-1/n}. \quad (7)$$

As shown in Fig. 3, this generalized index when calculated at low Reynolds numbers, namely k_0 , can be consistently correlated with intrinsic properties of the fluid and porous medium by means of the following semi-empirical expression [26, 28]:

$$k_0 = \frac{12}{25} \frac{n (75 k_r)^{1/n}}{3n+1} \frac{d_e^{(n-1)/n}}{3^{(n+1)/n}} \varepsilon^{2(1-n)/n} K^{(n-1)/n}, \quad (8)$$

where d_e is the only fitting parameter corresponding to an average effective pore diameter, namely, the average pore size (in units of d_p) of the system calculated as if it was a packed bed consisting of identical spheres [26, 29]. The parameter k_r corresponds to the value of k_D calculated for a Newtonian fluid ($n = 1$) under very low Reynolds conditions, i.e., the porous medium permeability according to Darcy's law.

In order to substantiate the non-Newtonian aspect of the fluid, it is also necessary to redefine the Reynolds number as [29],

$$Re_n \equiv \frac{k_0^n \rho u_0^{2-n}}{2 K^n d_p} \frac{1-\varepsilon}{\varepsilon^3}, \quad (9)$$

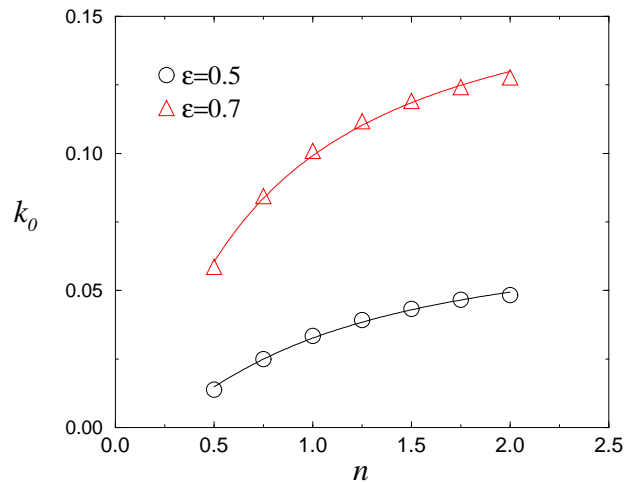


FIG. 3: (Color online) Dependence of the hydraulic conductivity at very low Reynolds numbers k_0 on the power-law exponent n for two different values of porosity ε . The solid lines are the least-squares fits to the simulation data using Eq. (8) with $d_e/d_p = 0.35$ and 1.58 , for $\varepsilon = 0.5$ and 0.7 , respectively.

where the term $(1 - \varepsilon)/\varepsilon^3$ has been adapted from the classical Kozeny-Carman equation [1]. It is worth mentioning that Eq. (9) breaks down close to the critical percolation porosity [30].

In the main plot of Fig. 2, we show that all data sets of k_n/k_0 against Re_n , with k_0 obtained from Eq. (8), collapse onto a single curve for the entire range of (modified) Reynolds numbers, independent of the numerical values of ε and n . Despite the details of the model porous medium geometry employed here as well as the complexity of the fluid rheology, this remarkable invariance of behavior suggests that the resulting flow properties of the system remain in the same universality class of Newtonian fluid flow in disordered porous media.

Next we present results for flow through three-dimensional porous media of Bingham fluids with rheology given approximately by the Herschel-Bulkley model Eq. (6). The proper way to quantify inertial and viscous forces in this case is to define the Reynolds number as $Re_B \equiv \rho u_0 d_p / K_B$. In Fig. 4 we show that the linear hydraulic conductivity, defined as $k_B \equiv K_B u_0 L / \Delta p$, remains constant up to a certain crossover that is proportional to the threshold τ_0 , $Re_x \sim \tau_0$. Below this crossover, since the fluid has Newtonian behavior with high viscosity μ_0 everywhere in the pore space, the flow can be macroscopically described by Darcy's law. Above this crossover, the presence of low and high strain rates zones in the flow leads to a nonuniform spatial distribution of fluid viscosity, therefore increasing the overall permeability index k_B of the system. This behavior persists up to the point in which inertial forces become relevant. While the specific fluid rheology investigated here tends to enhance the flow at high Re_B , the effect

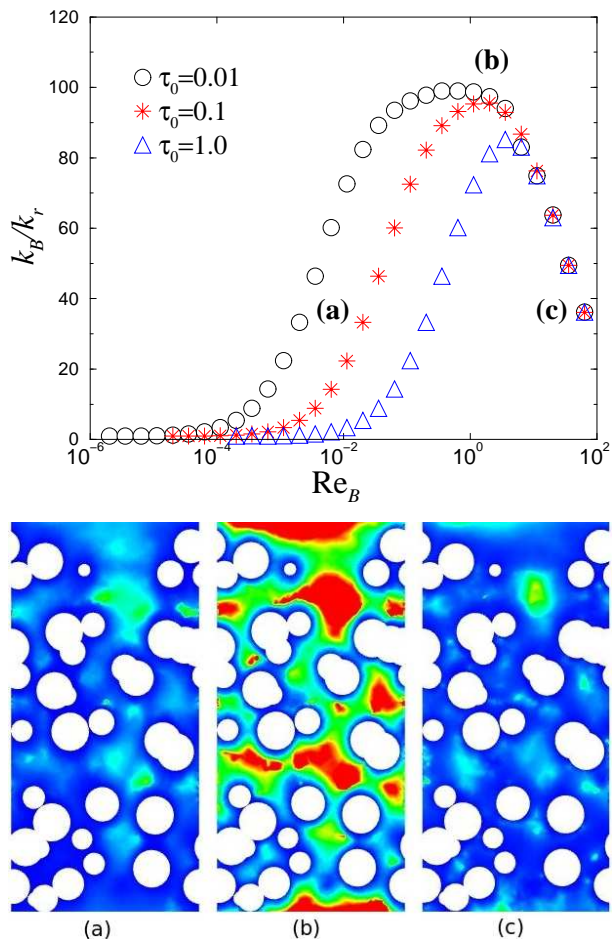


FIG. 4: (Color online) Flow of Bingham fluids (Herschel-Bulkley model) through three-dimensional porous media. The plot shows the variation of the ratio k_B/k_r with Reynolds number Re_B for different values of the parameter τ_0 , as defined in Eq. (6). Here k_r corresponds to the lower limit of k_B at very low Reynolds conditions. The presence of maxima in all cases is a distinctive result of the competition between rheology and convective non-linearities. The contour plots in (a), (b) and (c) show the spatial variation of the magnitude of the local ratio $|\vec{u}|/|\nabla p|$ calculated on the cross-section through the middle of the porous medium parallel to the flow, for $\tau = 0.1$ and $Re_B = 3.5 \times 10^{-2}$, 1.7 and 35, respectively. Their colors ranging from blue (dark) to red (light) correspond to low and high values of $|\vec{u}|/|\nabla p|$, respectively.

of inertia is to reduce the permeability index under the same conditions [7, 10]. As a result of this competition, a maximum hydraulic conductivity can be observed at an intermediate value of Re_B that is also dependent on the threshold τ_0 . As shown in Fig. 4, this effect is better illustrated when we observe contour plots of the local ratio $|\vec{u}|/|\nabla p|$ calculated at the middle cross-section of the porous medium. To the best of our knowledge, this condition of “enhanced flow” through disordered porous media represents a novel regime of momentum transport that could have potential applications in practical prob-

lems, e.g., chemical reactors, chromatographic columns and switches for flow. Finally, at sufficiently large values of Re_B , the viscosity of the fluid is uniform and therefore the local permeabilities become all the same, regardless of the value of Re_B and τ_0 . In this situation, all curves of k_B collapse.

Summarizing, in spite of the non-linear nature of the fluid rheology and the complex geometry of the interstitial pore volume, in the case of power-law fluids, we have shown the remarkable fact that the flow behavior can still be quantified in terms of an universal curve extending over a broad range of Reynolds conditions and power-law exponents. Our results for Bingham fluids are even more striking. There the pore space geometry, fluid rheology and inertia can combine to generate a particular condition of “enhanced transport” which should be found in experiments.

We thank CNPq, CAPES, FUNCAP, FINEP, Petrobras, the National Institute of Science and Technology for Complex Systems, and the Swiss National Science Foundation (SNF) under Grante No. 116052 for financial support.

-
- [1] F.A.L. Dullien, *Porous Media - Fluid Transport and Pore Structure* (Academic, New York, 1979).
 - [2] P.M. Adler, *Porous Media: Geometry and Transport* (Butterworth-Heinemann, Stoneham MA, 1992).
 - [3] M. Sahimi, *Flow and Transport in Porous Media and Fractured Rock* (VCH, Boston, 1995).
 - [4] A. Canceliere *et al.*, Phys. Fluids A **2**, 2085 (1990).
 - [5] S. Kostek, L.M. Schwartz, and D.L. Johnson, Phys. Rev. B **45**, 186 (1992).
 - [6] N.S. Martys, S. Torquato, and D.P. Bentz, Phys. Rev. E **50**, 403 (1994).
 - [7] J.S. Andrade *et al.*, Phys. Rev. E. **51**, 5725 (1995).
 - [8] A. Koponen, M. Kataja, and J. Timonen, Phys. Rev. E **56**, 3319 (1997).
 - [9] S. Rojas and J. Koplik, Phys. Rev. E **58**, 4776 (1998).
 - [10] J.S. Andrade *et al.*, Phys. Rev. Lett. **82**, 5249 (1999).
 - [11] D.A. Edwards *et al.*, Phys. Fluids **2**, 45 (1990).
 - [12] D.R. Koch and A.J.C. Ladd, J. Fluid Mech. **349**, 31 (1997).
 - [13] D.L. Mattson *et al.*, Am. J. Physiol. Regul. Integr. Comp. Physiol. **264**, 578 (1993).
 - [14] W.D. McCain *The properties of petroleum fluid* (Tulsa, Pennwel, 1990).
 - [15] A. Maestro, C. Gonzalez and J.M. Gutierrez, J. Rheol. **46**, 1445 (2002).
 - [16] M.J. Decker *et al.*, Comp. Sci. Tec. **67**, 565 (2007).
 - [17] A.B. Metzner, Adv. Chem. Eng. **1**, 77 (1956).
 - [18] M. Sahimi, AIChE J. **39**, 369 (1993).
 - [19] R.P. Chhabra, J. Comiti and I. Machac, Chem. Eng. Sci. **56**, 1 (2001).
 - [20] C.D. Lorenz and R.M. Ziff, J. Chem. Phys. **114**, 3659 (2001).
 - [21] W.H. Herschel and R. Bulkley, (1926), Kolloid Zeitschrift **39**, 291 (1926).

- [22] H.S. Tang, D.M. Kalyon, *Rheologica Acta* **43**, 80 (2004).
- [23] S.V. Patankar, *Numerical Heat Transfer and Fluid Flow* (Hemisphere, Washington DC, 1980); The FLUENT (trademark of FLUENT Inc.) fluid dynamics analysis package has been used in this study.
- [24] H.G. Weller, G. Tabor, H. Jasak and C. Fureby, *Computers in Physics* **12**, 620 (1998); The OpenFOAM®(Open Field Operation and Manipulation) software has been used in this study.
- [25] J.S. Andrade *et al.*, *Phys. Rev. Lett.* **98**, 194101 (2007).
- [26] R.B. Bird, W.E. Stewart and E.N. Lightfoot, *Transport Phenomena* (Wiley, New York, 2007).
- [27] R.G. Larson, *Ind. Eng. Chem. Fund.* **20**, 132 (1981).
- [28] C.B. Shah and Y.C. Yortsos, *AIChE J.* **41**, 1099 (1995).
- [29] R.H. Christopher and S. Middleman, *Ind. Eng. Chem. Fundam.* **4**, 422 (1965).
- [30] M. Sahimi, *Applications of Percolation Theory* (Taylor & Francis, London, 1994).